Jurnal Teknologi, 34(A) Jun 2001: 1–15

A NUMERICAL STUDY OF AIR FLOW IN A COAXIAL PIPE

ADI SURJOSATYO & FARID NASIR ANI*

Abstract. A simulation study of a cold-flow in coaxial pipes was carried out with varying drive-pipe diameter and entrance displacement (ΔL). The current work has studied the effect of the temperature of the entrance flow inlet with variation of ΔL to the entrained flow characteristics. To predict these flow characteristics, a numerical method was employed by the differencing scheme for integrating the continuity equation and energy equation. A k-ε turbulent model was used to simulate the turbulent transport quantities. The 2-D flow pattern was created as the result of using Fluent version 4.4 CFD modeling package. Results showed that increasing the air entrained temperature until 600 K would decrease the airflow rate. It was found that the diameter ratio of 2.81 has the highest entrained flow rate.

NOMENCLATURE

A	inflow area, m^2
C_{v1}	constant of proportionality (= 0.09)
$C_{1\varepsilon}$	empirical constants (= 1.44)
$C_{2\varepsilon}$	empirical constants (= 1.92)
dv	element of volume, m^3
h_c	average heat transfer coefficient, W/m °C
i, j	direction of flow
g	standard gravity acceleration (= 9.807 m/s^2)
J'	diffusion flux of the species j'
G_k	the rate of production of turbulent kinetic energy, kg/m s^3
G_b	generation of turbulence due to buoyancy, kg/m s^2
G_r	Grashof number
k	turbulent kinetic energy, m^2/s^2
k_c	molecular conductivity, W/m °C
k_t	effective conductivity due to turbulence transport ($k_t=c_p\mu_t/Pr_t$)
l_ε	mixing length scale, m
m	volumetric flow rate, kg/s
P	mean pressure, Pa
p_{op}	operating pressure, Pa
R	gas constant, 8.31434 kJ/kmol K
R_e	Reynold number

* Faculty of Mechanical Engineering, Universiti Teknologi Malaysia, 81310 Skudai, Johor Darul Takzim, Malaysia.

S_h term including heat of chemical reaction, any interphase exchange of heat, any other volumetric heat sources
T_a ambient temperature, K
T_f temperature reference, K
t velocity flow time, s
U, V mean velocity components in the direction of (X,Y), m/s
v inflow velocity, m/s
u', v' fluctuating components velocity in the direction of (X,Y), m/s
β coefficient of volume expansion, 1/K

$$= \frac{1}{v}\left(\frac{\partial v}{\partial T}\right)_p = -\frac{1}{\rho}\left(\frac{\partial \rho}{\partial T}\right)_p$$

$\overline{u'u'}$ Reynold stresses, m^2/s^2
$\overline{u'v'}$ Reynold stresses, m^2/s^2
$\overline{v'v'}$ Reynold stresses, m^2/s^2
ρ density, kg/m^3
δ_{ij} wall shear layer thickness, m
σ_k "Prandtl" numbers governing the turbulent diffusion of k and ε, (= 1.0)
σ_ε Prandt numbers governing the turbulent diffusion of k and ε, (= 1.3)
μ turbulent viscosity is proportional to the product of a turbulent velocity scale and length scale, $N.s/m^2$
υ kinematic viscosity, m^2/s
ε distribution of dissipation rate of k, m^2/s^3

1.0 INTRODUCTION

Ejectors are apparatus which entrained the low pressure gas by high pressure gas by interchanging the momentum of high speed driving gas discharged through a nozzle (or nozzles) with momentum of low pressure entrained gas around the driving jet (or jets). Ejectors usually consist of a nozzle (or nozzles) and a diffuser. That is, it has no moving part such as a rotor or piston. One of the advantages of ejector is that it is simple in construction and can compress a large flow rate of driving gas for a small and simple size ejector design as shown in Figure 1.

There are other names for having the same working principles, such as jet pump, injector and eductor. The general name for these systems is jet apparatus. The names mentioned above are distinguished according to the kinds, states and properties such as compressibility (gas, liquid, mixture of liquid and solid, mixture of gas, liquid and solid) of the driving and entrained fluids. Based on the normal ejector design the present study is to obtain some data for the design of the subsonic air in a coaxial pipe configuration.

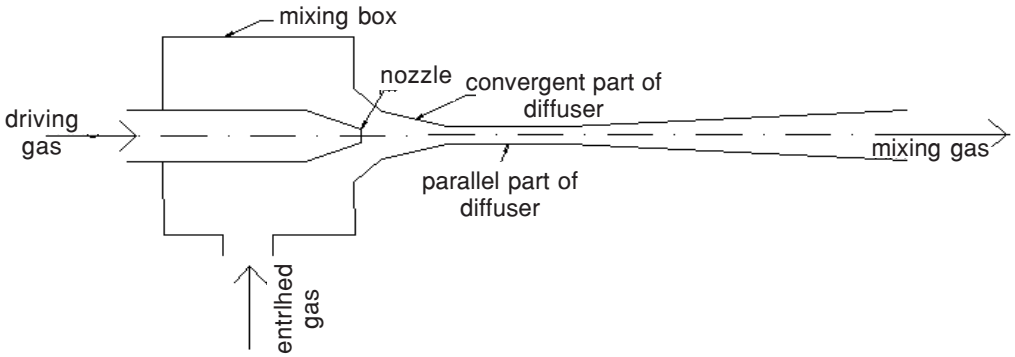

Figure 1 Ejector configuration

A research on ejector by Johannesen [1] reported features of ejector driven by and entraining compressible fluids. These include the aerodynamics of flow in the actuating nozzle, mixing chamber and the supersonic and subsonic diffusers. In general, the emphasis was made on the steam driven air ejector and experiments were made on such ejectors covering a range of geometrical proportions and pressure ratios.

A one dimensional method of analysis of air ejector was presented by Keenan *et al.* [2]. The analysis considers mixing of the primary and secondary streams at constant pressure and constant area and it was concluded that better performance would result from constant-pressure mixing. It should be noted, however, that while experimental verification of the analysis of constant area is well established, the other side, the lack of an appropriate design of constant-pressure mixing chamber has prevented from demonstrating the calculated supremacy of this ejector design.

Many of the previous studies dealt with single and multiple nozzle ejector. In the implementation of these designs should have a high air compression (≥ 2 bars) to have a sufficient entrained air. In the present work, another type of a simple ejector in the form a pair of coaxial pipe has been developed, which could work at low air compression (≤ 2 bars). The objective of present study is to simulate an ejector, which can deal with compressible gases as the driving gas and entrained gas. One of the merits is that it could use a blower with low power and entrained gas can occur which matches a specially fixed application.

2.0 THE AIR EJECTOR MODEL

Figure 2 shows the air-flow and configuration of the coaxial pipes. The primary air or driving air is introduced into the inlet pipe I which has the function of a nozzle. It is expected that due to pressure drop at outlet pipe I, an entrained flow can be created in the pipe II. The pipe II at this condition has the function of a diffuser.

In this model the length of driving pipe or pipe I is 665 mm and the length of entrain ejector pipe is 650 mm. The pipe entrance displacement starts from (ΔL = 50 mm

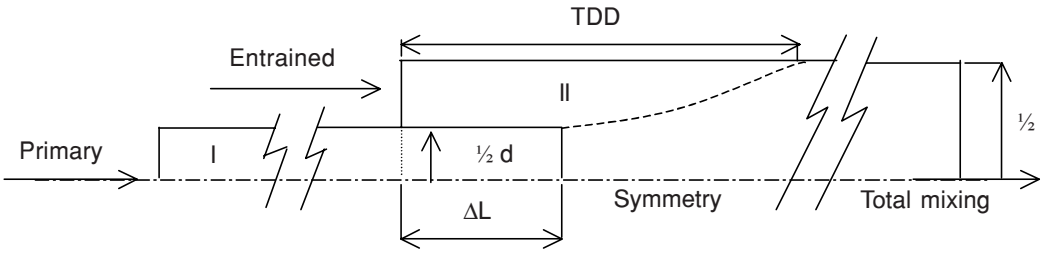

Figure 2 Air flow and ejector – drive pipes

(0.050 m) and it increased until (ΔL = 420 mm (0.420 m). Diameter Ratio (DR) is the diameter ratio of entrain ejector pipe to the drive pipe. The size of entrain ejector diameter are varied while the drive pipe diameter is constant. The Diameter Ratio (DR) used are 1.63, 2.34, 2.62 and 2.81. In this model, it is assumed that there is no friction on the pipe surface. Therefore, the effect of wall roughness is assumed negligible.

I : driving pipe; ΔL : pipe entrance displacement; TDD : Touch Down Distance
II : entrained pipe; D, d : entrain and drive pipe diameters; DR : Diameter Ratio (D/d)

3.0 GOVERNING EQUATIONS

The physical model considered in this work is shown schematically in Figure 2. This configuration is a two dimensional turbulent flow coaxial pipe. The governing Reynolds-averaged Navier Stokes equations for unsteady-state turbulent flow of two-dimensional [3–5] are as follows:

Continuity Equations:

Compressible fluid:

$$\frac{\partial \rho}{\partial t} + \frac{\partial (\rho U)}{\partial X} + \frac{\partial (\rho V)}{\partial Y} = 0 \tag{1}$$

Momentum Equations:

$$\rho \frac{\partial U}{\partial t} + \rho U \frac{\partial U}{\partial X} + \rho V \frac{\partial U}{\partial Y} = -\frac{\partial P}{\partial X} + \frac{\partial}{\partial X}\left(\nu \frac{\partial U}{\partial X}\right) + \frac{\partial}{\partial Y}\left(\nu \frac{\partial U}{\partial Y}\right) + \frac{\partial}{\partial X}\left(-\overline{u'u'}\right) + \frac{\partial}{\partial Y}\left(-\overline{u'u'}\right) \tag{2}$$

$$\rho\frac{\partial V}{\partial t}+\rho U\frac{\partial V}{\partial X}+\rho V\frac{\partial V}{\partial Y}=-\frac{\partial P}{\partial Y}+\frac{\partial}{\partial X}\left(v\frac{\partial V}{\partial X}\right)+\frac{\partial}{\partial Y}\left(v\frac{\partial V}{\partial Y}\right)+\frac{\partial}{\partial X}\left(-\overline{u'v'}\right)+\frac{\partial}{\partial Y}\left(-\overline{v'v'}\right) \tag{3}$$

The two Equations, equations (2) and (3) derived from Newton's Second Law, describe the conservation of momentum in the flow. The terms on the left-hand side of each of these equations describe acceleration term, the second and third terms being the convection terms, then the right hand side terms come from the pressure gradient in the flow and the effects of viscosity. The last two terms are the Reynold stresses, which represent the model to account for the effects of turbulence. These momentum equations govern the time-averaged properties of the flow.

The Turbulence Models

To solve Equations (1) to (3), a turbulence model for the turbulent transport quantities has to be specified. In the present work, the standard k-ε model [3–4, 6] based on Boussineq hypothesis is adopted. The local mean state of turbulence can be characterized by the turbulent kinetic energy k and its dissipation rate ε according to:

$$\rho\,\overline{u_i'u_j'}=\rho\frac{2}{3}k\delta_{ij}-v\left(\frac{\partial u_i}{\partial x_j}+\frac{\partial u_j}{\partial x_i}\right)+\frac{2}{3}v\frac{\partial u_i}{\partial X_i}\delta_{ij} \tag{4}$$

where $k = \frac{1}{2}\sum_i u_i'^2$ (5)

$v = \rho C_{\upsilon 1}\frac{k^2}{\varepsilon}$ (6)

$e = k^{2/3}/1_e$ (7)

Transport Equation for k and e

The values of k and e Equation (6) are obtained by solution of conservation energy:

$$\frac{\partial}{\partial t}(\rho k)+\frac{\partial}{\partial X_i}(\rho u_i k)=\frac{\partial}{\partial X_i}\left(\frac{\upsilon}{\sigma_k}\frac{\partial k}{\partial X_i}\right)+G_k+G_b-\rho\varepsilon \tag{8}$$

$$\frac{\partial}{\partial t}(\rho\varepsilon)+\frac{\partial}{\partial X_i}(\rho u_i\varepsilon)=\frac{\partial}{\partial X_i}\left(\frac{\upsilon}{\sigma_\varepsilon}\frac{\partial\varepsilon}{\partial X_i}\right)+C_{1\varepsilon}\frac{\varepsilon}{k}\left(G_k+(1-C_{3\varepsilon})G_b\right)-C_{2\varepsilon}\rho\frac{\varepsilon^2}{k} \quad (9)$$

where $$G_k=\upsilon\left(\frac{\partial u_j}{\partial X_i}+\frac{\partial u_i}{\partial X_j}\right)\frac{\partial u_j}{\partial x_j} \quad (10)$$

$$G_b=-g_i\frac{\upsilon}{\rho\sigma_h}\frac{\partial\rho}{\partial X_i} \quad (11)$$

The Effects of Turbulence on Heat Transfer

A theoretical correlation is based on the conservation of energy, which can predict the heat transfer process within the fluid and/or within solid in the model [3]. The simulation model solves the energy equation in the form of a transport equation for the static enthalpy, h:

$$\frac{\partial}{\partial t}(\rho h)+\frac{\partial}{\partial X_i}(\rho u_i h)=\frac{\partial}{\partial X_i}\left(k_c+k_t\frac{\partial T}{\partial X_i}\right)-\frac{\partial}{\partial X_i}\sum_j h_{j'}J_{j'}+\frac{\partial p}{\partial t}+\tau_{ik}\frac{\partial U_i}{\partial X_k}+S_h \quad (12)$$

Enthalpy h is defined as:

$$h=\sum_j m\,h_{j'} \quad (13)$$

where: $h_j=\int_{T_{\text{ref}}}^{T} c_{p,j'}\,dT$

4.0 NUMERICAL METHOD

The commercial software package, Fluent version 4.4, developed by Fluent Inc. was used as the primary source code for the model. This package employs a control volume-based or finite volume solution technique to allow full characterization of the flow field. The Navier-Stokes equations coupled with the Reynolds-averaged governing differential equations of continuity, energy, and species are solved in a discritized form. The standard k-ε turbulence model is employed. To obtain values at control volume interfaces needed for flux calculations, the power law interpolation scheme is utilised. The pressure-linked continuity and momentum equations are solved using the Semi-Implicit Method for Pressure-Linked Equations Consistent (SIMPLEC) solution algorithm. Specific details regarding convergence parameters such as multi-grid and under relaxation factors are available in Fluent. The convergence criterion is speci-

fied as the relative difference of every dependent variable between iteration steps being smaller than 10^{-6}. The pipes in the present work are assumed to be circular.

5.0 FLOW CONDITIONS OF SIMULATION

A simulation of subsonic air ejector was implemented to obtain an optimum condition of air flowrate in a pair of coaxial pipe. The simulations were carried out using a CFD software package. The flow conditions of simulation are as follows:

- subsonic and compressible air flow
- turbulence method: k-ε model
- boundary conditions:
  (i) inlet pressure as primary air at inside-pipe: 2 bars,
  (ii) inlet pressure where the secondary air or entrance air is induced: 1 bar (atmospheric pressure),
  (iii) outlet pressure at the outlet pipe where the exit of total air flow takes place: 1 bar (atmospheric pressure),
- 2 D flow assumption.

6.0 RESULTS AND DISCUSSIONS

Effect of Variation of Diameter Ratio on Air Velocity and Air Flowrate

Figure 3 and Figure 4 show the graphs of Air Velocity (AV) and Air Flowrate (AF) versus displacement. Each of the Figures has two curves, namely, primary (driving air) and entrained air flow. The primary air flow is kept constant. The displacement of entrance pipe has not influenced the primary air flowrate. This is due to enough high the pressure intake is compared to the pipe resistance, but for the entrained air flow there is a reduction for both air velocity and flowrate. The increase of pipe displacement means increase of flow path. Therefore, the area of entrained air flow is more restricted and the flow path for the entrained air has more resistance. From the graph, the highest entrained air flow is achieved at 0.05 m distance at the first drive-pipe displacement.

Figures 5 and 6 show the effect of Diameter Ratio variation on entrained air flowrate. As shown in Figure 5, the increase of DR has caused an increase of entrained mass flowrate.

To explain this observation, it is considered the following continuity equation:

$$\frac{\partial}{\partial t}\int \rho dv + \int \rho v.dA = 0 \tag{14}$$

Assumed the flow is steady, therefore the first term is zero $\left(\frac{\partial}{\partial t}\int \rho dv = 0\right)$, hence:

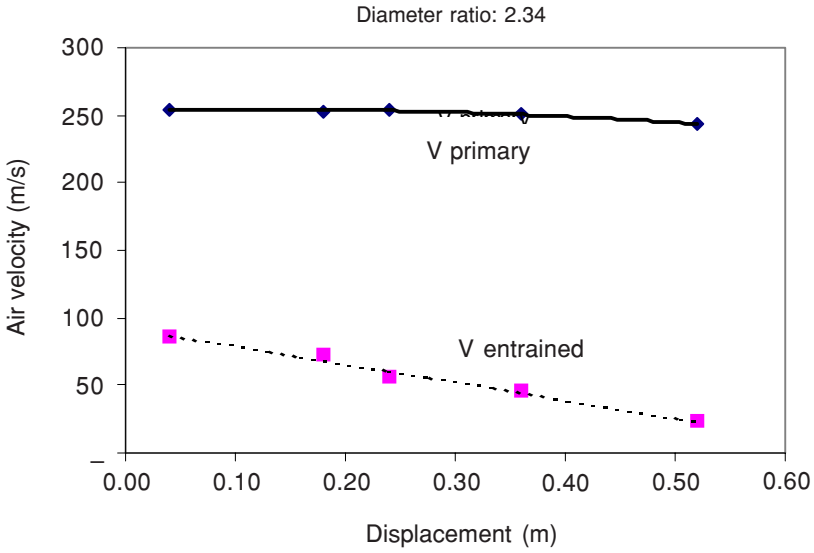

Figure 3 Effect of pipe displacement on air velocity

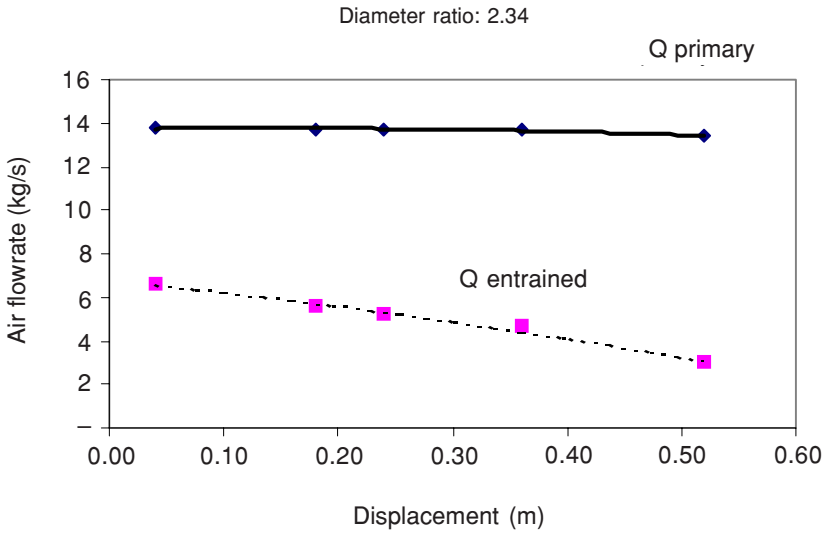

Figure 4 Effect of pipe displacement on air flow rate

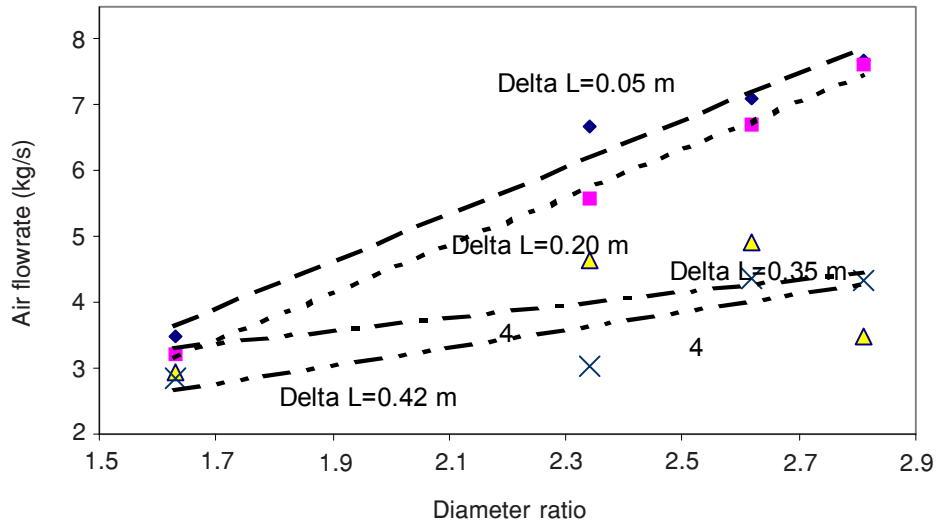

Figure 5 Entrained air flowrate versus Diameter Ratio

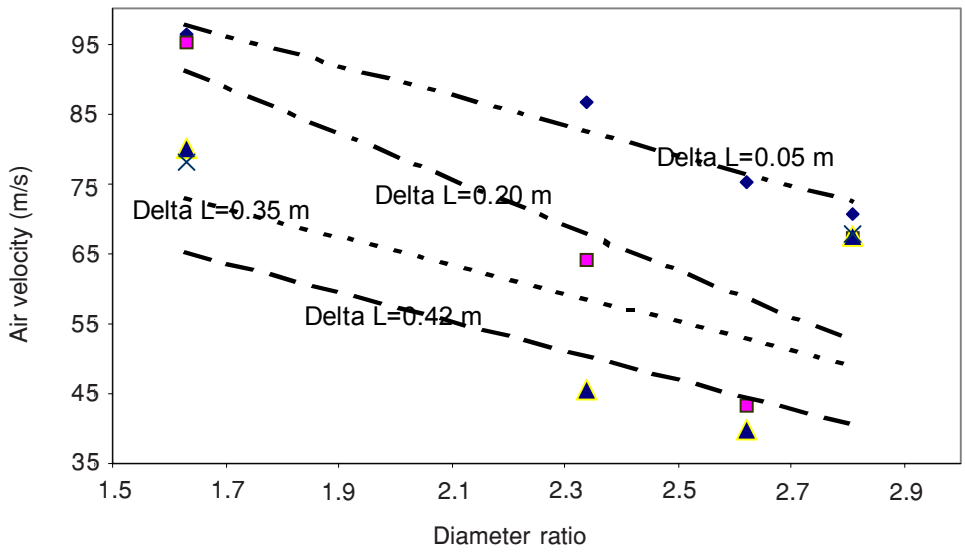

Figure 6 Entrained air velocity versus Diameter Ratio

$$\int \rho v.dA = 0 \tag{15}$$

Since, there is no flow through the wall and the flow is compressible, the equation (15) changed into a simplified form:

$$\rho_1 V_1 A_1 = \rho_2 V_2 A_2 = m \tag{16}$$

According to the equation (16), with the increase of DR, the area of flow is also increase, so the volumetric flow rate also increase as shown in figure 5 and air flow velocity decrease as shown in figure 6.

Effect of Diameter Ratio and Drive Pipe Displacement on Touch Down Distance (TDD)

Figures 7 and 8 show the graphs of the effect of both diameter ratio and drive pipe displacement ($\Delta L \approx$ Delta L) on Touch Down Distance (TDD). Touch Down Distance is a distance to begin of the fully developing zone. In these graphs three curves were plotted. Diameter Ratio (DR) 1.63, 2.34 and 2.62 have created the touch down distance, except for the highest displacement ΔL 0.420 m. In this displacement there is no touch down point on the entrain pipe and it has created turbulence effect on the outlet section of the entrain pipe since TDD is beyond the length of the pipe. Consequently, this condition can cause a flow resistance. The TDD have a tendency to increase for higher DR. Figure 7 shows the smallest TDD is achieved by the smallest displacement. Also increasing the entrance displacement ΔL causes the TDD to increase also as shown in Figure 8. It should be noted that there is a correlation between the entrained mass air flowrate and TDD. The entrained flow has created turbulent flow in such away that it has affected the friction flow with the primary flow. Higher entrained flow has caused a higher friction flow. This friction flow has a resistance to develop a reattachment zone. A slower of creating the reattachment zone therefore can influence a higher TDD.

Effect of Variation of Gas Temperature on Entrained Air Flowrate and Air Velocity

Figure 9 to Figure 12 show graphs of entrained air flowrate and air velocity at different ambient temperatures of the inlet secondary pipe (entrance pipe). These figures show that the increase of air temperatures of 300, 500 and 600°C at different Diameter Ratio DR of 1.63, 2.34, 2.62 and 2.81. Based on the simulation result, this configuration has influenced the different of air flowrate and velocity. The increase of gas temperature has affected the increase of entrained air velocity, but however, there is a decrease in entrained air flowrate.

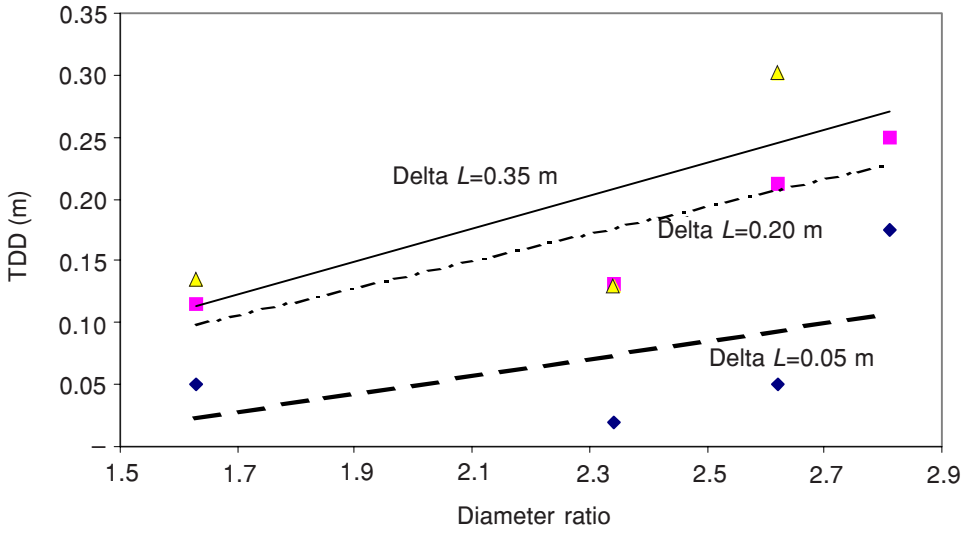

Figure 7 Touch down distance versus Diameter Ratio

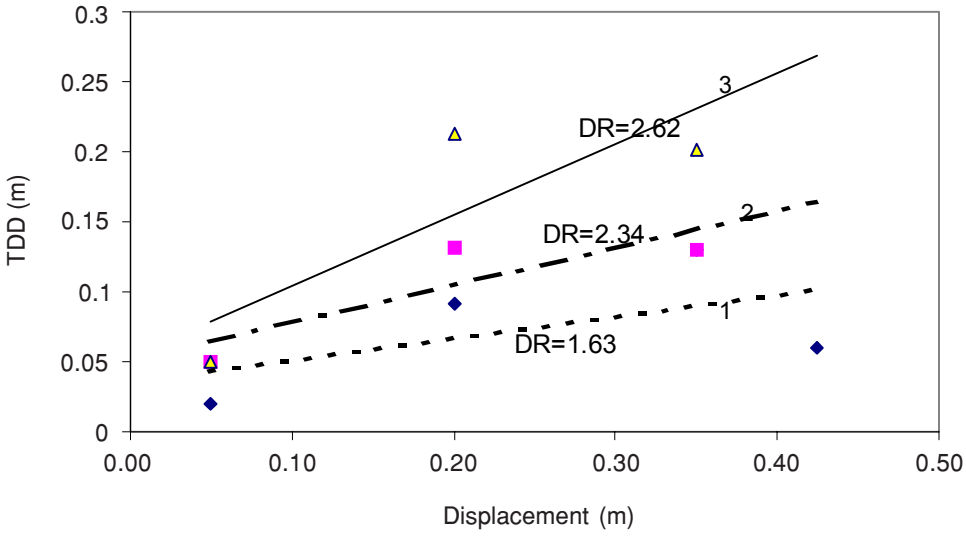

Figure 8 Touch down distance versus Displacement

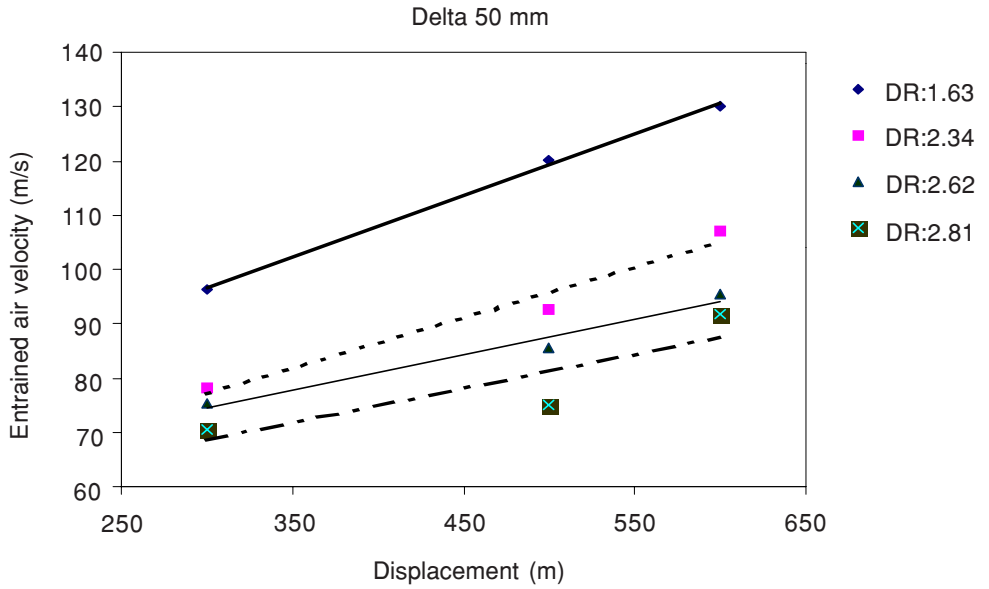

Figure 9 Diameter ratio versus entrained air velocity

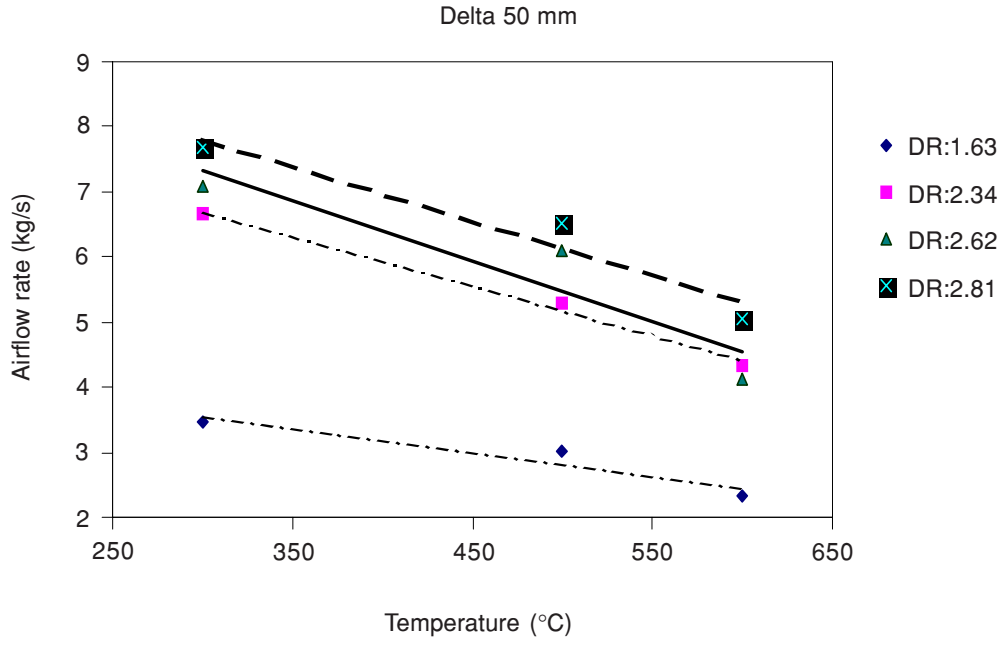

Figure 10 Temperature versus entrained airflow rate

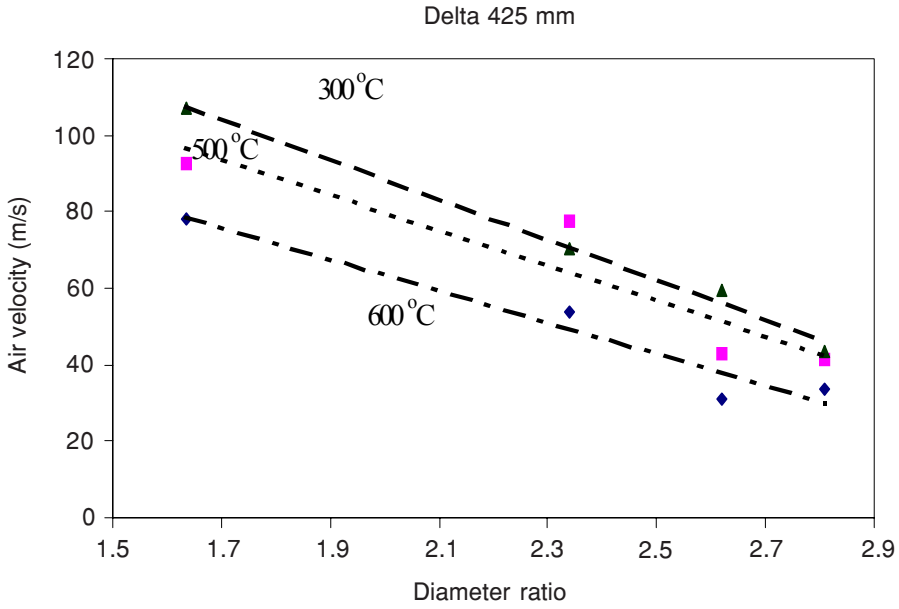

Figure 11 Diameter ratio versus entrained airflow

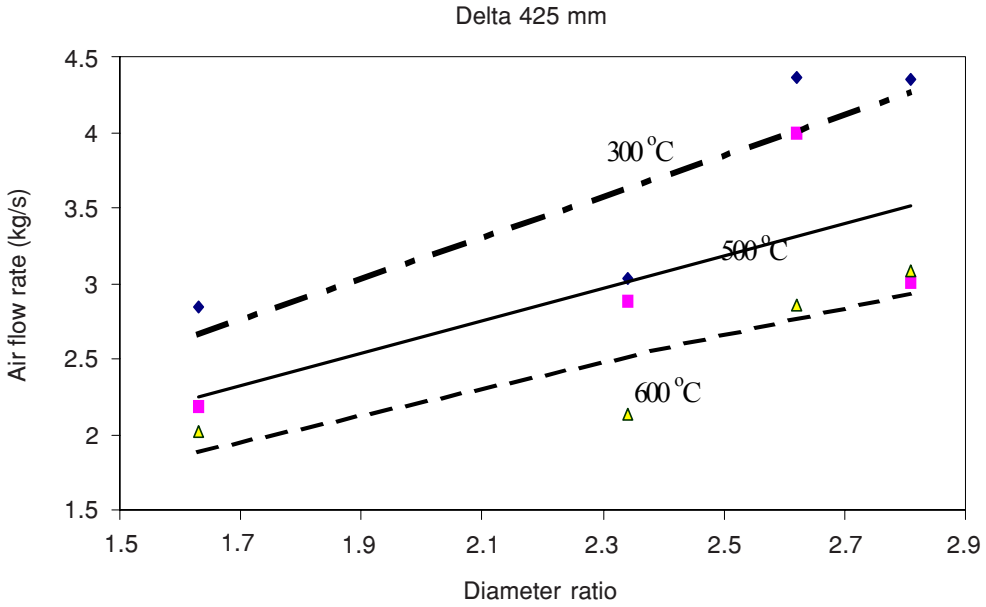

Figure 12 Diameter ratio versus entrained air flowrate

Holman [7] has studied the properties of air at atmospheric pressure. This study shows the value of air density and specific heat, which has a correlation with different air temperature. Equation 17 shows that the increase of air temperature affects the decrease of air density and increase of specific heat. This equation, which is indicated as the gas law [3, 7–8] shows the correlation between air density and the temperature as follow:

$$\rho = p_{op}/RT_a \tag{17}$$

If the temperature increases, the air density should decrease. Based on the continuity equation, the decrease of density affected the decrease of the air flowrate. Based on energy equation as stated in Equation 13, increasing the air temperature has the effect on increment of specific heat capacity value c_p [9]. To balance the total heat capacity of the system, the mass flowrate should decrease.

The increase in temperature also affects the air velocity. When the system changes from some initial velocity v_1 to a velocity v_2, the corresponding change in kinetic energy is [7]:

$$\Delta E = KE_2 - KE_1 = \int_{v_1}^{v_2} \frac{m}{g_c} v\, dv = \frac{1}{2g_c} m\left(v_2^2 - v_1^2\right) \tag{18}$$

The conservation of energy shows that when the temperature in a system is increased the heat Q in the system will also increase. This means, that there is a change in the internal energy ΔE. The work W is altered according to the energy equation by the amount of heat energy added Q, thus:

$$Q + W = DE \tag{19}$$

This indicates that

Energy added to system = accumulation of energy in the system.

In the present work there is no work W or $W = 0$, thus Equation (19) becomes

$$Q = \Delta E \tag{20}$$

where $Q = h_i = \int_{T_{\text{ref}}}^{T} c_{p,i}\, dT.$

7.0 CONCLUSIONS

(i) The Diameter Ratio (DR) of 1.63 has the smallest flow area, there is the lowest entrained air flow rate. This indicates that there is a correlation be-

tween entrained mass flow rate and Touch Down Distance (TDD). Thus, if the entrained air flow is low then Touch Down Distance is short.

(ii) Increase of the pipe displacement creates more resistant which causes the reduction of air velocity or air flowrate.

(iii) Touch Down Distance is influenced by two conditions i.e., displacement due to pipe resistant, and diameter ratio as well as flow area which has relationship with mass air flowrate.

(iv) The gas law and energy law are important equations to explain the correlation between air velocity and air flowrate with the variation of gas temperature.

(v) For each diameter ratio increasing of Diameter Ratio will increase the air flowrate, but the entrance pipe displacement will decrease the entrained rate.

(vi) Increasing the temperature until 600 K will decrease the air flow rate and the diameter ratio of 2.81 has the highest entrained flowrate.

ACKNOWLEDGMENT

The authors are grateful to RMC (Research Management Centre) UTM for supporting this research.

REFERENCES

[1] Johannesen, N. H. 1951. Ejector Theory and Experiments. *Danish Acad. Tech. Sci*. No.1: 176.
[2] Keenan, L. H., E. P. Neumann and F. P. Lustwerk. 1950. An Investigation of Ejector Design by Analysis and Experiment. *J. Appl. Mech*. 17(3).
[3] Fluent User's Guide. May 1997. *Fluent 4.4*. Vol. 1, 3 and 4.
[4] Shaw, C. T. 1989. *Computational Fluid Dynamic*. Longman.
[5] Patankar, S. V. 1980. *Numerical Heat Transfer and Fluid Flow*. Hemisphere Publishing Corporation.
[6] Launder, B. E. and D. B. Spalding. 1972. *Lectures in Mathematical Models of Turbulence*. London: Academic Press.
[7] Holman, J. P. 1993. *Thermodynamics*. McGraw-Hill International Book Company.
[8] Streeter, V. L. 1983. *Fluid Mechanics*. McGraw-Hill International Book Company.
[9] Cengel, Y. 1998. *Heat Transfer: A Practical Approach*. McGraw Hill.